

# Attractive $N$ - $\phi$ Interaction and Two-Pion Tail from Lattice QCD near Physical Point

Yan Lyu,<sup>1,2,\*</sup> Takumi Doi,<sup>2,†</sup> Tetsuo Hatsuda,<sup>2,‡</sup> Yoichi Ikeda,<sup>3,§</sup>  
 Jie Meng,<sup>1,4,¶</sup> Kenji Sasaki,<sup>3,\*\*</sup> and Takuya Sugiura<sup>2,††</sup>

<sup>1</sup>State Key Laboratory of Nuclear Physics and Technology,  
 School of Physics, Peking University, Beijing 100871, China

<sup>2</sup>Interdisciplinary Theoretical and Mathematical Sciences Program (iTHEMS), RIKEN, Wako 351-0198, Japan

<sup>3</sup>Center for Infectious Disease Education and Research, Osaka University, Suita 565-0871, Japan

<sup>4</sup>Yukawa Institute for Theoretical Physics, Kyoto University, Kyoto 606-8502, Japan

(Dated: May 24, 2022)

First results on the interaction between the  $\phi$ -meson and the nucleon ( $N$ ) are presented based on the  $(2+1)$ -flavor lattice QCD simulations with nearly physical quark masses. Using the HAL QCD method, the spacetime correlation of the  $N$ - $\phi$  system in the spin  $3/2$  channel is converted into the  $N$ - $\phi$  scattering phase shift through the interaction potential. The  $N$ - $\phi$  potential appears to be a combination of a short-range attractive core and a long-range attractive tail. The latter is found to be consistent with the two-pion exchange (TPE) obtained from the interaction between a color-dipole and the nucleon. The resultant scattering length and effective range for  $m_\pi = 146.4$  MeV are  $a_0^{(3/2)} = -1.43(23)_{\text{stat.}} \left( \begin{smallmatrix} +36 \\ -06 \end{smallmatrix} \right)_{\text{syst.}}$  fm and  $r_{\text{eff}}^{(3/2)} = 2.36(10)_{\text{stat.}} \left( \begin{smallmatrix} +02 \\ -48 \end{smallmatrix} \right)_{\text{syst.}}$  fm, respectively. The magnitude of the scattering length is shown to have non-trivial dependence of  $m_\pi$  and is sensitive to the existence of the long-range tail from TPE.

*Introduction.*— The interaction between vector mesons and the nucleon ( $N$ ) is one of the most fundamental quantities to study the meson properties in nuclear matter and the modification of QCD condensates at finite baryon density [1]. Among others, the  $\phi$ -meson attracts particular interest, since the interactions of the  $s\bar{s}$  pair with the nucleon and nucleus are not well understood at low energies.

Experimentally, the production and absorption of the  $\phi$ -meson in nuclear matter has been actively studied through photon and proton( $p$ )-induced reactions with various nuclear targets (Spring8-LEPS [2], KEK-PS E325 [3], JLab-CLAS [4], and COSY-ANKE [5]) as summarized in Ref. [6]. Recently, the ALICE Collaboration at LHC presented a new result on the  $p$ - $\phi$  interaction through the femtoscopic analysis of the  $p$ - $\phi$  pair produced in the  $pp$  reaction: They reported a spin-averaged scattering length  $a_{p\phi} = -0.85(34)_{\text{stat.}}(14)_{\text{syst.}}$  fm [7], an order of magnitude larger than that obtained from the photo-production data by the CLAS Collaboration at JLab [8] combined with the vector meson dominance [9].

Theoretically, the properties of the  $\phi$ -meson in nuclear matter and its relation to the in-medium  $s\bar{s}$  condensate have been extensively discussed [10–13]. The microscopic origin of the force between  $\phi$  and  $N$  is also an important open problem. In particular, the two-pion exchange (TPE) as the major long-range contribution between a color-dipole and the nucleon [14] is of strong relevance to this problem and will shed new light on the important role of pion dynamics in hadron interactions.

Under these experimental and theoretical circumstances, it is most desirable to carry out realistic lattice QCD simulations of the  $N$ - $\phi$  interaction. In this Letter,

we report a first simulation of the  $N$ - $\phi$  system in a large lattice volume  $\simeq (8.1 \text{ fm})^3$  with light dynamical quarks near the physical point. We focus on the highest-spin  $N$ - $\phi$  system, the  ${}^4S_{3/2}$  channel, with the notation  ${}^{2s+1}L_J$  ( $s$  = total spin,  $L$  = orbital angular momentum,  $J$  = total angular momentum). This is because its coupling to two-body open channels  $\Lambda K({}^2D_{3/2})$  and  $\Sigma K({}^2D_{3/2})$  are kinematically suppressed at low energies due to their  $D$ -wave nature, similar to the situation for the highest-spin  $N$ - $\Omega$  system (the  ${}^5S_2$  channel) [15]. Moreover, decay processes with three or more particles in the final state such as  $\Sigma\pi K$ ,  $\Lambda\pi K$ , and  $\Lambda\pi\pi K$  are expected to be suppressed due to the small phase space. Indeed, we will show below that visible effects from such decays cannot be seen from our lattice data in the  ${}^4S_{3/2}$  channel. By using the HAL QCD method [16–18], which converts the spacetime correlation of hadrons to the physical observables, we obtain the  $N$ - $\phi$  scattering phase shift, the  $S$ -wave scattering length  $a_0^{(3/2)}$  and the effective range  $r_{\text{eff}}^{(3/2)}$  in the  ${}^4S_{3/2}$  channel. (For recent applications of the HAL QCD method to the baryon-baryon interactions, see Refs. [15, 19–21].)

*HAL QCD Method.*— Thanks to the Haag-Nishijima-Zimmermann reduction formula for composite particles [22], the interaction between hadrons can be extracted as the energy-independent non-local potential  $U(\mathbf{r}, \mathbf{r}')$  [16]. Such a potential can be defined from the normalized four-point function,

$$\begin{aligned}
 R(\mathbf{r}, t) &= \frac{\sum_{\mathbf{x}} \langle 0 | N(\mathbf{r} + \mathbf{x}, t) \phi(\mathbf{x}, t) \bar{\mathcal{J}}(0) | 0 \rangle}{\sqrt{Z_\phi Z_N} e^{-(m_N + m_\phi)t}} \\
 &= \sum_n a_n \psi_n(\mathbf{r}) e^{-(\Delta E_n)t} + O(e^{-(\Delta E^*)t}). \quad (1)
 \end{aligned}$$

Here the energy eigenvalue and the energy shift of each elastic scattering state are given by  $E_n = \sqrt{m_N^2 + \mathbf{k}_n^2} + \sqrt{m_\phi^2 + \mathbf{k}_n^2}$  and  $\Delta E_n = E_n - (m_N + m_\phi)$ , respectively, with  $\mathbf{k}_n$  being the relative momentum in the center of mass frame. The equal-time Nambu-Bethe-Salpeter wave function for each eigenstate is denoted by  $\psi_n(\mathbf{r})$ . The wave function renormalization constant for  $\phi$  ( $N$ ) is given by  $Z_\phi$  ( $Z_N$ ). The contributions from the inelastic scattering states are exponentially suppressed as  $O(e^{-(\Delta E^*)t})$  with  $\Delta E^*$  being the energy of the inelastic threshold relative to  $m_N + m_\phi$ . The overlapping factor between the  $N$ - $\phi$  source operator  $\bar{\mathcal{J}}(0)$  and the  $n$ -th eigenstate  $|n\rangle$  is given by  $a_n = \langle n | \bar{\mathcal{J}}(0) | 0 \rangle$ . The wall-type operator with the Coulomb gauge fixing is used for the source, while the local operators are adopted for the sink,

$$\begin{aligned} N_\alpha(x) &= \epsilon_{abc} \left[ u^{aT}(x) C \gamma_5 d^b(x) \right] u_\alpha^c(x), \\ \phi_i(x) &= \delta_{ab} \bar{s}^a(x) \gamma_i s^b(x). \end{aligned} \quad (2)$$

Here  $a, b$ , and  $c$  are the color indices,  $i$  is the vector index,  $\alpha$  is the Dirac index restricted to the upper two components,  $C = \gamma_4 \gamma_2$  is the charge conjugation, and  $T$  denotes the transposition for the Dirac index. Misner's method of approximate partial wave decomposition on a cubic grid, originally developed in the field of numerical relativity [23], is used to make the  $S$ -wave projection on the lattice [24]. The normalized four-point functions  $R(\mathbf{r}, t)$  with the spin projection onto the states with  $J = 3/2$  are used to extract the potential.

It has been shown that  $R(\mathbf{r}, t)$  satisfies the integro-differential equation [17],

$$\begin{aligned} & \left[ \frac{1 + 3\delta^2}{8\mu} \frac{\partial^2}{\partial t^2} - \frac{\partial}{\partial t} - H_0 + O(\delta^2 \partial_i^3) \right] R(\mathbf{r}, t) \\ &= \int d\mathbf{r}' U(\mathbf{r}, \mathbf{r}') R(\mathbf{r}', t), \end{aligned} \quad (3)$$

with  $H_0 = -\nabla^2/(2\mu)$ ,  $\mu = m_N m_\phi / (m_N + m_\phi)$  being the reduced mass,  $\delta = (m_N - m_\phi) / (m_N + m_\phi)$  being the mass asymmetry. We have neglected the term of  $O(\delta^2 \partial_i^3)$  in the above, since it is found to be consistent with zero within the statistical error in our simulation. In practical calculations, a derivative expansion of the non-local potential is employed;  $U(\mathbf{r}, \mathbf{r}') = V(r) \delta(\mathbf{r} - \mathbf{r}') + \sum_{n=1} V_n(\mathbf{r}) \nabla^n \delta(\mathbf{r} - \mathbf{r}')$ . Then, the leading-order central potential  $V(r)$  reads,

$$V(r) = R^{-1}(\mathbf{r}, t) \left[ \frac{1 + 3\delta^2}{8\mu} \frac{\partial^2}{\partial t^2} - \frac{\partial}{\partial t} - H_0 \right] R(\mathbf{r}, t). \quad (4)$$

The truncation error of the derivative expansion is found to be small at low energies by using the method of finite volume spectra analysis [25, 26] (Fig. S1 in the Supplemental Material).

*Lattice setup.*— The  $(2 + 1)$ -flavor gauge configurations are generated with the Iwasaki gauge action at  $\beta = 1.82$

and the nonperturbatively  $O(a)$ -improved Wilson quark action with stout smearing at nearly physical quark masses [27]. The lattice spacing is  $a \simeq 0.0846$  fm ( $a^{-1} \simeq 2333$  MeV), and the lattice volume is  $L^4 = 96^4$ , corresponding to  $La \simeq 8.1$  fm. The isospin-averaged masses of  $\pi$ ,  $K$ ,  $\phi$ , and  $N$  from the single-state fitting in the interval  $t/a = 15$ -25 for the mesons and 11-18 for the nucleon are listed in Table I with statistical errors in the parentheses. Corresponding experimental values [28] are shown in the third column. The lattice results are about 6% larger than the experimental values for the pseudo-scalar mesons, while about 3% (2%) larger for  $\phi$  ( $N$ ). With our light quark masses slightly heavier than the physical masses,  $\phi$  is below the  $K\bar{K}$  threshold, which prohibits a fall-apart decay of  $\phi$ .

TABLE I. Isospin-averaged hadron masses with statistical errors obtained from  $(2+1)$ -flavor lattice QCD simulations together with the experimental values.

Hadron	Lattice [MeV]	Expt. [MeV]
$\pi$	146.4(4)	138.0
$K$	524.7(2)	495.6
$\phi$	1048.0(4)	1019.5
$N$	954.0(2.9)	938.9

We use 200 configurations separated by 10 trajectories. For each configuration, the forward and backward propagations are averaged, the hypercubic symmetry on the lattice (4 rotations) is utilized, and 80 measurements are performed by shifting the source position in a temporal direction in order to reduce the statistical fluctuation. In total, the number of measurements is 128000. With the periodic boundary condition for all directions, the quark propagators are calculated by the domain-decomposed solver [29], and the hadron correlation functions are obtained by the unified contraction algorithm [30]. The contraction diagram with the pair annihilation of  $s\bar{s}$  is not considered, since it is known to be small, e.g. less than 0.4% correction to the  $\phi$ -meson mass [31]. The statistical errors are evaluated by the jackknife method with a bin size of 20 configurations throughout this Letter. A comparison with a bin size of 40 configurations shows that the bin size dependence is small.

*Numerical results.*— The  $N$ - $\phi$  potential  $V(r)$  in the  ${}^4S_{3/2}$  channel defined in Eq. (4) with the lattice measurement of  $R(\mathbf{r}, t)$  is shown in Fig. 1 for Euclidean times,  $t/a = 12, 13$ , and 14. (See Fig. S2 in the Supplemental Material for the  $t$ -dependence of  $V(r)$  in a wider range of  $t$ .) These Euclidean times are chosen such that they are large enough to suppress contaminations from excited states in the single-hadron correlator and simultaneously small enough to avoid exponentially increasing statistical errors. The potentials from different  $t$  agree with each other within statistical errors, which indicates that the  $N$ - $\phi$  correlation function is dominated by the elastic scattering states in the  ${}^4S_{3/2}$  channel; we do not find the

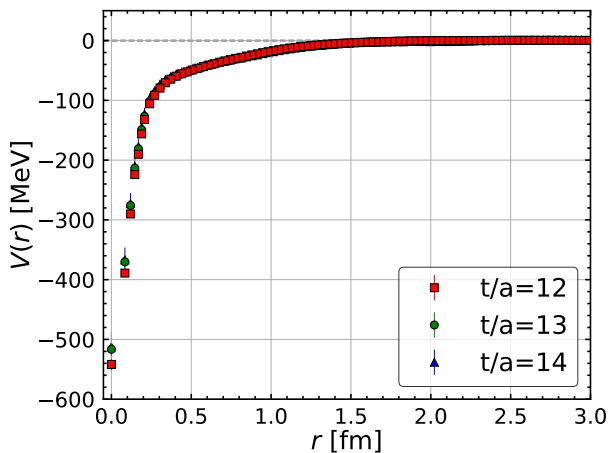


FIG. 1. (Color online). The  $N$ - $\phi$  potential  $V(r)$  in the  ${}^4S_{3/2}$  channel as a function of separation  $r$  at Euclidean time  $t/a = 12$  (red squares), 13 (green circles) and 14 (blue triangles).

effects of the two-body open channels ( $\Lambda K({}^2D_{3/2})$  and  $\Sigma K({}^2D_{3/2})$ ) as well as the three-body open channels including  $N\phi \rightarrow \{\Sigma^*K, \Lambda(1405)K\} \rightarrow \{\Lambda\pi K, \Sigma\pi K\}$ . This is in sharp contrast to the  ${}^2S_{1/2}$  case where we found that the  $N$ - $\phi$  potential shows a clear  $t$ -dependence, as expected from the  $S$ -wave fall-apart decay into  $\Lambda K({}^2S_{1/2})$  and  $\Sigma K({}^2S_{1/2})$ .

The potential  $V(r)$  in the  ${}^4S_{3/2}$  channel shown in Fig. 1 is attractive for all distances and has a characteristic two-component structure, the attractive core at short distance and the attractive tail at long distance, similar to the case of the  $N\Omega({}^5S_2)$  potential [15]. We note that the Pauli exclusion principle between quarks, which partially gives rise to the repulsive core in the  $NN$  interaction [32, 33], does not operate in the present case, since  $N$  and  $\phi$  have no common valence quarks.

As has been discussed for the interaction between color dipoles [34–36], non-perturbative gluon exchange is expected to appear in the form of the TPE at long distance. The idea was generalized to the interaction between a color-dipole and the nucleon with the result,  $V(r \gg (2m_\pi)^{-1}) = -\alpha \frac{\exp(-2m_\pi r)}{r^2}$ , where  $\alpha$  is proportional to  $m_\pi^4$  [14]. To check such a long distance behavior of  $V(r)$ , we show in Fig. 2 the spatial effective energy,  $E_{\text{eff}}(r) = -\frac{\ln[-V(r)r^2/\alpha]}{r}$ , as a function of  $r$  with  $\alpha \simeq 91 \text{ MeV} \cdot \text{fm}^2$  determined by fitting the lattice data of  $V(r)$  at long distance. We find that  $E_{\text{eff}}(r)$  has a plateau at  $2m_\pi = 292.8 \text{ MeV}$  for  $r > 1.0 \text{ fm}$ , which indicates that the long-range part of the  $N$ - $\phi$  potential is indeed dominated by the TPE.

In order to convert the potential to physical observables, we perform an uncorrelated fit of the lattice QCD

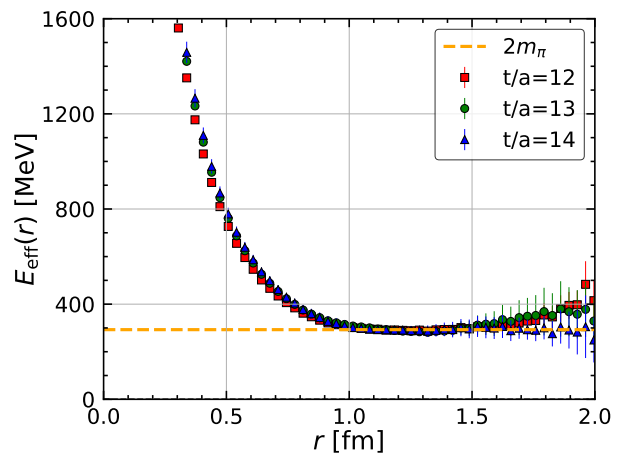


FIG. 2. (Color online). The spatial effective energy  $E_{\text{eff}}(r)$  as a function of separation  $r$  at Euclidean time  $t/a = 12$  (red squares), 13 (green circles) and 14 (blue triangles). The orange dashed line corresponds to  $2m_\pi$  with lattice pion mass  $m_\pi = 146.4 \text{ MeV}$ .

potential by using two different functional forms,

$$\begin{aligned} \text{A: } V_{\text{fit}}(r) &= \sum_{i=1,2} a_i e^{-(r/b_i)^2} + a_3 m_\pi^4 f(r; b_3) \frac{e^{-2m_\pi r}}{r^2}, \\ \text{B: } V_{\text{fit}}(r) &= \sum_{i=1,2,3} a_i e^{-(r/b_i)^2}. \end{aligned} \quad (5)$$

The fit A is motivated by the TPE tail at long distance with an overall strength proportional to  $m_\pi^4$  [14], while the fit B is a purely phenomenological Gaussian form for comparison. In fit A, we consider two types of form factors commonly used in the  $NN$  potentials: (i) The Nijmegen-type form factor [37],  $f_{\text{erfc}}(r; b_3) = [\text{erfc}(\frac{m_\pi}{\Lambda} - \frac{\Lambda r}{2}) - e^{2m_\pi r} \text{erfc}(\frac{m_\pi}{\Lambda} + \frac{\Lambda r}{2})]^2 / 4$  with  $\Lambda = 2/b_3$  and the complementary error function  $\text{erfc}(x) = \frac{2}{\sqrt{\pi}} \int_x^\infty e^{-z^2} dz$ . This is motivated by the exponential-type regularization of the pion propagator in the momentum space,  $1/(k^2 + m_\pi^2) \rightarrow e^{-(k/\Lambda)^2}/(k^2 + m_\pi^2)$ . (ii) The Argonne-type form factor [38],  $f_{\text{exp}}(r; b_3) = (1 - e^{-(r/b_3)^2})^2$ . We refer to fit A with (i) and (ii) as fit A<sub>erfc</sub> and fit A<sub>exp</sub>, respectively. The pion mass in fit A<sub>erfc,exp</sub> is taken to be  $m_\pi = 146.4 \text{ MeV}$ , and the fit range is chosen as  $0 < r < 3.0 \text{ fm}$ . We found that the fit A<sub>erfc,exp</sub> and the fit B provide an equally good fit ( $\chi_{\text{d.o.f}}^2 = 0.3\text{-}0.4$ ) and are stable against the choice of  $t$ . In Table II, we show the fit results for  $t/a = 14$ , which are expected to have least contamination from the inelastic states. Changing the fit range of the potential to  $0.1 < r < 2.5 \text{ fm}$  does not affect the results within statistical errors. Also we found that the simple fitting functions such as the Yukawa form  $\sim -\frac{\exp(-\mu r)}{r}$  [39, 40] and the van der Waals (Casimir-Polder) form  $\sim -\frac{1}{r^k}$  with  $k = 6$  (7) [41] cannot reproduce the lattice data.

TABLE II. The fit parameters in Eq. (5) with statistical errors quoted in the parentheses at  $t/a = 14$ . The fit range is  $0 < r < 3.0$  fm. In  $a_3 m_\pi^{4n}$ , we take  $n = 1$  and  $n = 0$  for fit A and B, respectively.  $A_{\text{erfc}}$  ( $A_{\text{exp}}$ ) denotes fit A with the Nijmegen-type (Argonne-type) form factor.

fit	$A_{\text{erfc}}$	$A_{\text{exp}}$	B
$a_1$ [MeV]	-376(20)	-371(27)	-371(19)
$b_1$ [fm]	0.14(1)	0.13(1)	0.15(3)
$a_2$ [MeV]	306(122)	-119(39)	-50(35)
$b_2$ [fm]	0.46(4)	0.30(5)	0.66(61)
$a_3 m_\pi^{4n}$ [MeV·fm $^{2n}$ ]	-95(13)	-97(14)	-31(53)
$b_3$ [fm]	0.41(7)	0.63(4)	1.09(41)

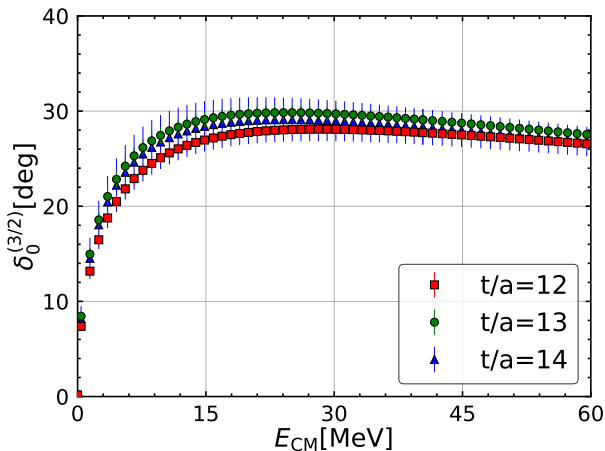


FIG. 3. The  $N$ - $\phi$  scattering phase shifts  $\delta_0^{(3/2)}$  in the  ${}^4S_{3/2}$  channel obtained from  $V_{\text{fit}}(r)$  at  $t/a = 12$  (red squares), 13 (green circles), and 14 (blue triangles).

Figure 3 shows the  $N$ - $\phi$  scattering phase shifts  $\delta_0^{(3/2)}$  in the  ${}^4S_{3/2}$  channel as a function of the center of mass kinetic energy  $E_{\text{CM}} = \sqrt{m_N^2 + k^2} + \sqrt{m_\phi^2 + k^2} - (m_N + m_\phi)$  obtained by using  $V_{\text{fit}}(r)$  with the fit  $A_{\text{erfc}}$ . The scattering phase shifts from different  $t$  are consistent with each other within statistical errors. The scattering length  $a_0^{(3/2)}$  and the effective range  $r_{\text{eff}}^{(3/2)}$  can be extracted from the effective range expansion for small  $k$  as  $k \cot \delta_0^{(3/2)}(k) = -\frac{1}{a_0^{(3/2)}} + \frac{1}{2} r_{\text{eff}}^{(3/2)} k^2 + O(k^4)$ . In Table III,  $a_0^{(3/2)}$  and  $r_{\text{eff}}^{(3/2)}$  are shown for the present pion mass  $m_\pi = 146.4$  MeV; the central values and the statistical errors are obtained from the data at  $t/a = 14$  with the fit  $A_{\text{erfc}}$ , while the systematic errors in the second parentheses are estimated by comparing results for  $t/a = 12$ -14 with  $A_{\text{erfc,exp}}$  and B. Other possible systematic errors are as follows; (i) the finite volume effect of the potential, which is expected to be small as  $\exp(-2m_\pi(L/2)a) \lesssim 0.3\%$  due to the large volume, and (ii) the finite cutoff effect, which is also expected to be small as  $O((a\Lambda_{\text{QCD}})^2) \sim O(1\%)$  due to the non-perturbative  $O(a)$ -improvement. As an alternative estimate, we study how much scattering parameters are

sensitive to the potential in short range, where the finite cutoff effect should be most prominent. It is found that  $a_0^{(3/2)}$  and  $r_{\text{eff}}^{(3/2)}$  change only  $\sim 2\%$  even when we completely cut the short-range potential at  $r < 0.1$  fm.

TABLE III. The scattering length  $a_0^{(3/2)}$  and the effective range  $r_{\text{eff}}^{(3/2)}$  obtained by using  $V_{\text{fit}}(r)$  at  $m_\pi = 146.4$  MeV with statistical and systematic errors. Estimated central values using a model-dependent extrapolation of  $V_{\text{fit}}(r)$  to  $m_\pi = 138.0$  MeV are also shown for comparison.

$m_\pi$ [MeV]	$a_0^{(3/2)}$ [fm]	$r_{\text{eff}}^{(3/2)}$ [fm]
146.4	$-1.43(23)_{\text{stat.}} \left( \begin{smallmatrix} +36 \\ -06 \end{smallmatrix} \right)_{\text{sys.}}$	$2.36(10)_{\text{stat.}} \left( \begin{smallmatrix} +02 \\ -48 \end{smallmatrix} \right)_{\text{sys.}}$
138.0	$\simeq -1.25$	$\simeq 2.49$

To estimate how the scattering parameters change toward the physical quark mass, we keep  $a_{1,2,3}$  and  $b_{1,2,3}$  in  $V_{\text{fit}}(r)$  fixed in fit  $A_{\text{erfc,exp}}$  and smoothly change the long-range potential by taking the isospin-averaged physical pion mass  $m_\pi = 138.0$  MeV in the region where the TPE is dominated ( $r > 1.0$  fm from Fig.2). By calculating the scattering phase shifts with such a potential with the physical masses of  $\phi$  and  $N$ , we obtain estimated values of  $a_0^{(3/2)}$  and  $r_{\text{eff}}^{(3/2)}$  for  $m_\pi = 138.0$  MeV in Table III. Although the range of the TPE is increased by the smaller pion mass, the characteristic  $m_\pi^4$  behavior of the TPE strength makes the overall attraction weaker. Note that this is only a model-dependent qualitative estimate and needs to be confirmed by future physical-point simulations.

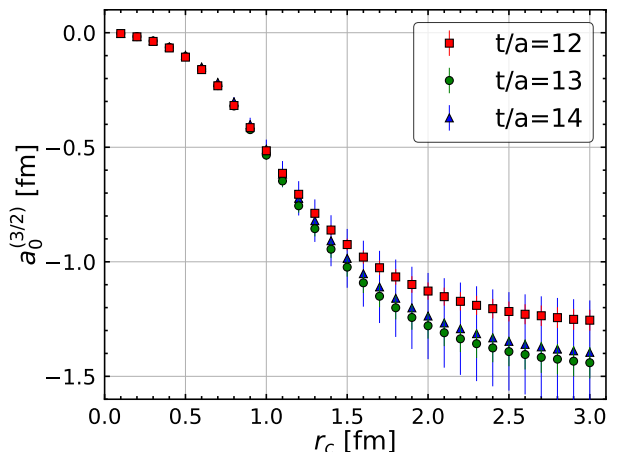


FIG. 4. The scattering length  $a_0^{(3/2)}$  obtained from  $V(r; r_c) = \theta(r_c - r)V_{\text{fit}}(r)$  as a function of cutoff length  $r_c$  at  $t/a = 12$  (red squares), 13 (green circles), and 14 (blue triangles).

Since we do not have reliable information on the  $N\phi({}^2S_{1/2})$  potential from lattice QCD at the moment due to the effect of the open channels, a comparison of our results with spin-averaged scattering parameters should be made with caution. With this reservation in mind,

our  $a_0^{(3/2)}$  is found to be one or two orders of magnitude larger than the previous theoretical results in QCD sum rules [42, 43]. Such a discrepancy may be due to the difficulty of obtaining the long-range TPE contribution from the low-order truncation of the operator product expansion in QCD sum rules. In fact, the magnitude of  $a_0^{(3/2)}$  becomes considerably smaller when the long-range potential is cut off. Shown in Fig. 4 is  $a_0^{(3/2)}$  as a function of cutoff length  $r_c$  obtained by the potential,  $V(r; r_c) = \theta(r_c - r)V_{\text{fit}}(r)$  with the fit  $A_{\text{erfc}}$ . Considerable decrease of  $|a_0^{(3/2)}|$  from 1.43 fm at  $r_c = \infty$  to about 0.1 fm at  $r_c = 0.5$  fm can be seen.

*Summary.*— In this Letter, we present a first lattice QCD calculation on the interaction of the  $N$ - $\phi$  system in the  ${}^4S_{3/2}$  channel based on the  $(2 + 1)$ -flavor simulations with nearly physical quark masses. The interaction potential in the  $N\phi({}^4S_{3/2})$  channel is extracted from lattice data of the hadronic spacetime correlation using the HAL QCD method. The potential is found to be attractive for all distances and appears to be a combination of an attractive core at short distances and a two-pion exchange (TPE) tail at long distances ( $r > 1$  fm). The latter is well fitted by the characteristic form of the TPE obtained by the interaction of a color-dipole and the nucleon. The scattering parameters obtained from our potential at  $m_\pi = 146.4$  MeV is summarized in Table III. By examining the potential fitted to the lattice data, we find that the scattering length  $a_0^{(3/2)}$  is sensitive to the length scale of  $r > 0.5$  fm. Also, we suggest that the  $N$ - $\phi$  attraction could be weaker at the physical pion mass due to the characteristic  $m_\pi^4$  dependence of the strength of the TPE.

Our  $a_0^{(3/2)}$  is substantially larger in magnitude than the previous calculations of the spin-averaged  $a_0$  using QCD sum rules but is comparable to the spin-averaged  $a_0$  by ALICE Collaboration within the error bar [7]. Also, our  $r_{\text{eff}}^{(3/2)}$  is about three times smaller than the spin-averaged  $r_{\text{eff}}$  by ALICE Collaboration. To make a firm comparison between theory and experiment, we need to perform a  $\Lambda K$ - $\Sigma K$ - $N\phi$  coupled-channel analysis to reveal the complex dynamics of the  ${}^2S_{1/2}$  and  ${}^4S_{3/2}$  channels as well as to perform physical-point simulations.

The present lattice QCD study near the physical point provides a first step to exploring the interaction of  $s\bar{s}$  with the nucleon from first principle. The heavier system such as  $c\bar{c}$  interacting with the nucleon pioneered in [44, 45] is also an important problem to be studied near the physical point.

*Acknowledgments.*— We thank members of the HAL QCD Collaboration for stimulating discussions. Y. L. thanks Xu Feng for the helpful discussions. We thank members of the PACS Collaboration for the gauge configuration generation conducted on the K computer at RIKEN. The lattice QCD measurements have been performed on Fugaku and HOKUSAI supercom-

puters at RIKEN. We thank ILDG/JLDG [46], which serves as essential infrastructure in this study. This work was partially supported by HPCI System Research Project (hp120281, hp130023, hp140209, hp150223, hp150262, hp160211, hp170230, hp170170, hp180117, hp190103, hp200130, hp210165, and hp210212), the National Key R&D Program of China (Contract Nos. 2017YFE0116700 and 2018YFA0404400), the National Natural Science Foundation of China (Grant Nos. 11935003, 11975031, 11875075, and 12070131001), the JSPS (Grant Nos. JP18H05236, JP16H03978, JP19K03879, JP18H05407, and JP21K03555), the MOST-RIKEN Joint Project “Ab initio investigation in nuclear physics”, “Priority Issue on Post-K computer” (Elucidation of the Fundamental Laws and Evolution of the Universe), “Program for Promoting Researches on the Supercomputer Fugaku” (Simulation for basic science: from fundamental laws of particles to creation of nuclei), and Joint Institute for Computational Fundamental Science (JICFuS).

---

\* helvetia@pku.edu.cn

† doi@ribf.riken.jp

‡ thatsuda@riken.jp

§ yikeda@cider.osaka-u.ac.jp

¶ mengj@pku.edu.cn

\*\* kenjis@cider.osaka-u.ac.jp

†† takuya.sugiura@riken.jp

- [1] R. S. Hayano and T. Hatsuda, *Rev. Mod. Phys.* **82**, 2949 (2010).
- [2] T. Ishikawa *et al.*, *Phys. Lett. B* **608**, 215 (2005), arXiv:nucl-ex/0411016.
- [3] R. Muto *et al.* (KEK-PS E325 Collaboration), *Phys. Rev. Lett.* **98**, 042501 (2007).
- [4] M. H. Wood *et al.* (CLAS Collaboration), *Phys. Rev. Lett.* **105**, 112301 (2010).
- [5] A. Polyanskiy *et al.*, *Phys. Lett. B* **695**, 74 (2011), arXiv:1008.0232 [nucl-ex].
- [6] L. Tolos and L. Fabbietti, *Prog. Part. Nucl. Phys.* **112**, 103770 (2020), arXiv:2002.09223 [nucl-ex].
- [7] S. Acharya *et al.* (ALICE Collaboration), *Phys. Rev. Lett.* **127**, 172301 (2021).
- [8] B. Dey, C. A. Meyer, M. Bellis, and M. Williams (CLAS), *Phys. Rev. C* **89**, 055208 (2014), [Addendum: *Phys. Rev. C* **90**, 019901 (2014)], arXiv:1403.2110 [nucl-ex].
- [9] I. I. Strakovsky, L. Pentchev, and A. Titov, *Phys. Rev. C* **101**, 045201 (2020), arXiv:2001.08851 [hep-ph].
- [10] T. Hatsuda and S. H. Lee, *Phys. Rev. C* **46**, R34 (1992).
- [11] M. Asakawa and C. M. Ko, *Nucl. Phys. A* **572**, 732 (1994).
- [12] P. Gubler and W. Weise, *Nucl. Phys. A* **954**, 125 (2016), arXiv:1602.09126 [hep-ph].
- [13] P. Gubler and D. Satow, *Prog. Part. Nucl. Phys.* **106**, 1 (2019), arXiv:1812.00385 [hep-ph].
- [14] J. Tarrús Castellà and G. a. Krein, *Phys. Rev. D* **98**, 014029 (2018), arXiv:1803.05412 [hep-ph].

- [15] T. Iritani *et al.* (HAL QCD), Phys. Lett. B **792**, 284 (2019), arXiv:1810.03416 [hep-lat].
- [16] N. Ishii, S. Aoki, and T. Hatsuda, Phys. Rev. Lett. **99**, 022001 (2007).
- [17] N. Ishii, S. Aoki, T. Doi, T. Hatsuda, Y. Ikeda, T. Inoue, K. Murano, H. Nemura, and K. Sasaki (HAL QCD Collaboration), Physics Letters B **712**, 437 (2012).
- [18] S. Aoki and T. Doi, Frontiers in Physics **8**, 307 (2020).
- [19] S. Gongyo, K. Sasaki, S. Aoki, T. Doi, T. Hatsuda, Y. Ikeda, T. Inoue, T. Iritani, N. Ishii, T. Miyamoto, and H. Nemura (HAL QCD Collaboration), Phys. Rev. Lett. **120**, 212001 (2018).
- [20] K. Sasaki *et al.* (HAL QCD Collaboration), Nucl. Phys. A **998**, 121737 (2020), arXiv:1912.08630 [hep-lat].
- [21] Y. Lyu, H. Tong, T. Sugiura, S. Aoki, T. Doi, T. Hatsuda, J. Meng, and T. Miyamoto, Phys. Rev. Lett. **127**, 072003 (2021), arXiv:2102.00181 [hep-lat].
- [22] W. Zimmermann, in *Wondering in the fields: Festschrift for Prof. K. Nishijima*, edited by K. Kawarabayashi and A. Ukawa (World Scientific, Singapore, 1987).
- [23] C. W. Misner, Class. Quant. Grav. **21**, S243 (2004), arXiv:gr-qc/9910044.
- [24] T. Miyamoto, Y. Akahoshi, S. Aoki, T. Aoyama, T. Doi, S. Gongyo, and K. Sasaki, Phys. Rev. D **101**, 074514 (2020).
- [25] T. Iritani, S. Aoki, T. Doi, T. Hatsuda, Y. Ikeda, T. Inoue, N. Ishii, H. Nemura, and K. Sasaki (HAL QCD Collaboration), JHEP **03**, 007 (2019), arXiv:1812.08539 [hep-lat].
- [26] Y. Lyu, H. Tong, T. Sugiura, S. Aoki, T. Doi, T. Hatsuda, J. Meng, and T. Miyamoto, Phys. Rev. D **105**, 074512 (2022).
- [27] K.-I. Ishikawa, N. Ishizuka, Y. Kuramashi, Y. Nakamura, Y. Namekawa, Y. Taniguchi, N. Ukita, T. Yamazaki, and T. Yoshie (PACS Collaboration), Proc. Sci. **LATTICE2015**, 075 (2016), arXiv:1511.09222 [hep-lat].
- [28] P. A. Zyla *et al.* (Particle Data Group), Progress of Theoretical and Experimental Physics **2020** (2020), 083C01.
- [29] K.-I. Ishikawa, I. Kanamori, H. Matsufuru, I. Miyoshi, Y. Mukai, Y. Nakamura, K. Nitadori, and M. Tsuji, “102 PFLOPS Lattice QCD quark solver on Fugaku,” (2021), arXiv:2109.10687 [hep-lat].
- [30] T. Doi and M. G. Endres, Comput. Phys. Commun. **184**, 117 (2013), arXiv:1205.0585 [hep-lat].
- [31] B. Chakraborty, C. T. H. Davies, G. C. Donald, J. Koponen, and G. P. Lepage (HPQCD Collaboration), Phys. Rev. D **96**, 074502 (2017), arXiv:1703.05552 [hep-lat].
- [32] T. Inoue, S. Aoki, T. Doi, T. Hatsuda, Y. Ikeda, N. Ishii, K. Murano, H. Nemura, and K. Sasaki (HAL QCD), Nucl. Phys. A **881**, 28 (2012), arXiv:1112.5926 [hep-lat].
- [33] M. Oka, K. Shimizu, and K. Yazaki, Prog. Theor. Phys. Suppl. **137**, 1 (2000).
- [34] G. Bhanot and M. E. Peskin, Nucl. Phys. B **156**, 391 (1979).
- [35] H. Fujii and D. Kharzeev, Phys. Rev. D **60**, 114039 (1999), arXiv:hep-ph/9903495.
- [36] N. Brambilla, G. a. Krein, J. Tarrús Castellà, and A. Vairo, Phys. Rev. D **93**, 054002 (2016), arXiv:1510.05895 [hep-ph].
- [37] V. G. J. Stoks, R. A. M. Klomp, C. P. F. Terheggen, and J. J. de Swart, Phys. Rev. C **49**, 2950 (1994), arXiv:nucl-th/9406039.
- [38] R. B. Wiringa, V. G. J. Stoks, and R. Schiavilla, Phys. Rev. C **51**, 38 (1995).
- [39] S. J. Brodsky, I. Schmidt, and G. F. de Téramond, Phys. Rev. Lett. **64**, 1011 (1990).
- [40] H. Gao, T.-S. H. Lee, and V. Marinov, Phys. Rev. C **63**, 022201 (2001).
- [41] T. Appelquist and W. Fischler, Physics Letters B **77**, 405 (1978).
- [42] Y. Koike and A. Hayashigaki, Prog. Theor. Phys. **98**, 631 (1997), arXiv:nucl-th/9609001.
- [43] F. Klingl, N. Kaiser, and W. Weise, Nucl. Phys. A **624**, 527 (1997), arXiv:hep-ph/9704398.
- [44] T. Kawanai and S. Sasaki, Phys. Rev. D **82**, 091501 (2010), arXiv:1009.3332 [hep-lat].
- [45] T. Sugiura, Y. Ikeda, and N. Ishii, PoS **LATTICE2018**, 093 (2019), arXiv:1905.02336 [nucl-th].
- [46] <http://www.lqcd.org/ildg> and <http://www.jldg.org>.

# Attractive $N$ - $\phi$ Interaction and Two-Pion Tail from Lattice QCD near Physical Point

## SUPPLEMENTAL MATERIAL

We present a detailed account of the systematics of the leading-order (LO) potential  $V(r)$  in this supplemental material.

We first consider the truncation error of the derivate expansion. For this purpose, we construct a Hamiltonian  $H$  in a three-dimensional lattice box with the LO potential  $V(r)$  [1, 2],

$$H = -\frac{\nabla^2}{2\mu} + V(r), \quad H\psi_n(\mathbf{r}) = \varepsilon_n\psi_n(\mathbf{r}). \quad (\text{S1})$$

Here  $\varepsilon_n$  is related to  $\Delta E_n = \sqrt{m_N^2 + 2\mu\varepsilon_n} + \sqrt{m_\phi^2 + 2\mu\varepsilon_n} - (m_N + m_\phi)$ . From the NBS wavefunction  $\psi_n(\mathbf{r})$ , one can construct an optimized sink operator as a projection to each  $n$ -th state,

$$S_n = \sum_{\mathbf{r}} \psi_n^\dagger(\mathbf{r}) \left[ \sum_{\mathbf{x}} N(\mathbf{r} + \mathbf{x}, t) \phi(\mathbf{x}, t) \right], \quad (\text{S2})$$

which is expected to overlap largely to the  $n$ -th state. The temporal correlation function with such an optimized sink operator can be obtained as,

$$R_n(t) = \sum_{\mathbf{r}} \psi_n^\dagger(\mathbf{r}) R(\mathbf{r}, t) = a_n e^{-(\Delta E_n)t} + O(e^{-(\Delta E^*t)}). \quad (\text{S3})$$

The effective energy for the  $n$ -th state can be defined from  $R_n(t)$  as,

$$\Delta E_n^{\text{eff}} = \frac{1}{a} \ln \left[ \frac{R_n(t)}{R_n(t+1)} \right]. \quad (\text{S4})$$

Thus, by comparing  $\Delta E_n$  from the LO potential  $V(r)$  and  $\Delta E_n^{\text{eff}}$  from the projected temporal correlation function, we can make a highly non-trivial check on the systematic errors in the LO potential  $V(r)$ .

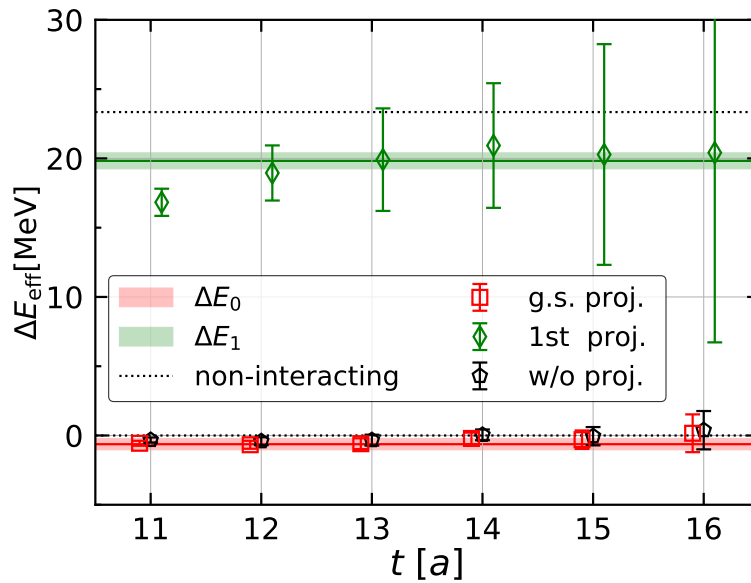


FIG. S1. The effective energies  $\Delta E_{0,1}$  from the LO potential  $V(r)$  (colored bands) and  $\Delta E_{0,1}^{\text{eff}}$  from the projected temporal correlation functions (colored points). Black pentagons represent the effective energy extracted from the temporal correlation function without projection, i.e.  $R(t) = \sum_{\mathbf{r}} R(\mathbf{r}, t)$ . The black dotted lines are  $\Delta E_{0,1}$  for a non-interacting system.

Shown in Fig. S1 are  $\Delta E_{0,1}$  from the LO potential  $V(r)$  (colored bands), and  $\Delta E_{0,1}^{\text{eff}}$  from the projected temporal correlation functions (colored points). We also show the effective energy from the temporal correlation function without projection, i.e.  $R(t) = \sum_r R(\mathbf{r}, t)$ , for comparison (black points). We found that  $\Delta E_{0,1}$  and  $\Delta E_{0,1}^{\text{eff}}$  are consistent with each other within statistical errors, which indicates that the systematic errors in the LO potential  $V(r)$  are well under control.

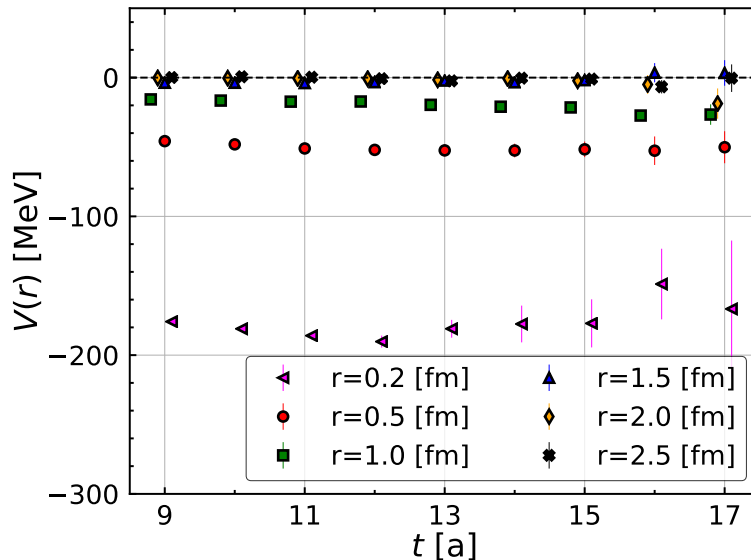


FIG. S2. The  $t$ -dependence of the  $N\phi$  potential  $V(r)$  in the  ${}^4S_{3/2}$  channel for several distances  $r$ . For visibility, data are a little shifted horizontally.

In Fig. S2, we show the  $t$ -dependence of  $V(r)$  for several distances  $r = 0.2, 0.5, 1.0, 1.5, 2.0,$  and  $2.5$  fm in a wide range of  $t$ ,  $9 \leq t/a \leq 17$ . We found the potential at given  $r$  varies slowly with  $t$ . This is a typical signal showing that the elastic scattering states in  $N\phi({}^4S_{3/2})$  play a dominant role at these Euclidean times. In other words, if  $N\phi({}^4S_{3/2})$  strongly couples to open channels such as  $\Lambda K({}^2D_{3/2})$ ,  $\Sigma K({}^2D_{3/2})$ ,  $\Lambda\pi K$ , and  $\Sigma\pi K$ , the potential at given  $r$  would decrease monotonically with  $t$  increasing.

\* helvetia@pku.edu.cn

† doi@ribf.riken.jp

‡ thatsuda@riken.jp

§ yiked@cidr.osaka-u.ac.jp

¶ mengj@pku.edu.cn

\*\* kenjis@cidr.osaka-u.ac.jp

†† takuya.sugiura@riken.jp

[1] T. Iritani, S. Aoki, T. Doi, T. Hatsuda, Y. Ikeda, T. Inoue, N. Ishii, H. Nemura, and K. Sasaki (HAL QCD Collaboration), JHEP **03**, 007 (2019), arXiv:1812.08539 [hep-lat].

[2] Y. Lyu, H. Tong, T. Sugiura, S. Aoki, T. Doi, T. Hatsuda, J. Meng, and T. Miyamoto, Phys. Rev. D **105**, 074512 (2022).